

Synthesis of metallic copper nanoparticles and metal-metal bonding process using them

Yoshio Kobayashi ^{*1}, Hiroaki Nakazawa ^{1a}, Takafumi Maeda ^{1b},
Yusuke Yasuda ^{2c} and Toshiaki Morita ^{2d}

¹ Department of Biomolecular Functional Engineering, College of Engineering, Ibaraki University,
4-12-1 Naka-narusawa-cho, Hitachi, Ibaraki 316-8511, Japan

² Hitachi Research Laboratory, Hitachi Ltd., 7-1-1 Omika-cho, Hitachi, Ibaraki 319-1292, Japan

(Received November 14, 2016, Revised April 03, 2017, Accepted May 29, 2017)

Abstract. Metallic copper nanoparticles were synthesised by reduction of copper ions in aqueous solution, and metal-metal bonding by using the nanoparticles was studied. A colloid solution of metallic copper nanoparticles was prepared by mixing an aqueous solution of CuCl₂ (0.01 M) and an aqueous solution of hydrazine (reductant) (0.2-1.0 M) in the presence of 0.0005 M of citric acid and 0.005 M of n-hexadecyltrimethylammonium bromide (stabilizers) at reduction temperature of 30-80°C. Copper-particle size varied (in the range of ca. 80-165 nm) with varying hydrazine concentration and reduction temperature. These dependences of particle size are explained by changes in number of metallic-copper-particle nuclei (determined by reduction rate) and changes in collision frequency of particles (based on movement of particles in accordance with temperature). The main component in the nanoparticles is metallic copper, and the metallic-copper particles are polycrystalline. Metallic-copper discs were successfully bonded by annealing at 400°C and pressure of 1.2 MPa for 5 min in hydrogen gas with the help of the metallic-copper particles. Shear strength of the bonded copper discs was then measured. Dependences of shear strength on hydrazine concentration and reduction temperature were explained in terms of progress state of reduction, amount of impurity and particle size. Highest shear strength of 40.0 MPa was recorded for a colloid solution prepared at hydrazine concentration of 0.8 M and reduction temperature of 50°C.

Keywords: metal nanoparticle; nano-particles; nanosized metals; chemical synthesis; nano-materials

1. Introduction

Metal-metal bonding is an indispensable process mainly in fields such as metalworking industry and electronics (Tu 2007, Shi *et al.* 1999, Darwish *et al.* 2000, Nami *et al.* 2010, Ji *et al.* 2012, Lee and Kwon 2013). Conventional metal-metal bonding is performed by pressurizing two or more metallic materials under annealing at high temperature (Weisman 1976, Nami *et al.* 2010, Duarte *et al.* 2012, Lee and Kwon 2013). During the bonding, components of one metal diffuse

*Corresponding author, Professor, E-mail: yoshio.kobayashi.yk@vc.ibaraki.ac.jp

^a Bachelor, E-mail: i-had-appendicitis-5years-ago@ezweb.ne.jp

^b Ph.D., E-mail: t.maeda0504@gmail.com

^c Ph.D., E-mail: yusuke.yasuda.jf@hitachi.com

^d Ph.D., E-mail: toshiaki.morita.sj@hitachi.com

into the other metal and, consequently, the metals are bonded. The high-temperature annealing promotes the diffusion. Because the high annealing temperature may damage the metals to be bonded, the annealing temperature should be lowered. It can be lowered by using a metallic solder or a metallic filler with a low melting point (Wang *et al.* 2012, Kotadia *et al.* 2014, Ji *et al.* 2015). Even at low temperature, the filler components diffuse into the metals intensively, so metal-metal bonding is achieved at low temperature. Because of its low melting point, tin-lead alloy is a representative filler used in metal-metal bonding. However, the bonded metals may be released on exposure to temperatures higher than their melting points due to re-melting of the alloy. Tin-lead alloy also faces the following problem. As several researchers suggested, the lead contained in the alloy is toxic to the human body (Abtewa and Selvaduray 2000, Kikuchi *et al.* 2001, Shiue *et al.* 2003, Noor *et al.* 2010, Kotadia *et al.* 2014, Zhang and Tu 2014), so its use tends to be limited. Various lead-free, tin-related alloys have also low melting points. In light of health and environmental concerns, metal-metal bonding processes using lead-free, tin-related alloys have been proposed. However, such alloys still face the problem derived from their low melting points.

Nanoparticles of metals have a total apparent surface area larger than that of their bulk; therefore, they can contact the other materials efficiently and effectively achieve metal-metal bonding. Nanoparticles have another advantage over their bulk; that is, in general, melting points of metals are decreased with decreasing nanoparticle size to the nanometer order (Shibuta and Suzuki 2010, Son *et al.* 2012, Hashimoto *et al.* 2012). Decreasing melting points in this manner can be applied to metal-metal bonding at low temperature.

Since metallic silver has high electrical conductivity, high thermal conductivity and chemical stability, its nanoparticles are a good candidate as a nanoparticle filler. Accordingly, utilizing metallic silver nanoparticles as filler has been studied (Ide *et al.* 2005, Bai *et al.* 2006, Murray *et al.* 2006, Yasuda *et al.* 2009, Morisada *et al.* 2010, Yan *et al.* 2012a). The silver-based nanoparticles exert excellent metal-metal bonding properties. However, their cost is higher than that of many other metals expected to function as a metallic nanoparticle filler. In addition, bonding with metallic-silver nanoparticles as a filler may deteriorate with time owing to electrochemical migration of the silver (Kim *et al.* 2013, Lu *et al.* 2015). Metallic copper is another candidate nanoparticle filler for bonding, since it also has excellent electrical and thermal conductivities, and is available at low cost if a method for producing metallic copper nanoparticles is simple and the obtained nanoparticles is chemically stable. In addition, the electrochemical migration of copper does not occur as easily as that of silver (Tan *et al.* 2012). Several methods for fabricating nanoparticles of metallic copper have been proposed (Niranjan and Chakraborty 2012, Argueta-Figueroa *et al.* 2014, Xu *et al.* 2015), and the works on the methods have been limited to development of a simple and easily reproducible way of preparing the nanoparticles, investigation of their potential use in dental materials, and continuous synthesis of the nanoparticles using microreactors. Metal-metal bonding using metallic copper nanoparticles has been extensively studied by several researchers (Morisada *et al.* 2010, Nishikawa *et al.* 2011, Yan *et al.* 2012b, Ishizaki *et al.* 2013). In their works, the metallic copper nanoparticles have been produced in organic solvents, which gives unsafety and high environmental load. From this view point, our research group has focused on preparation of chemically-stable metallic copper nanoparticles prepared in aqueous solution, and studied on metal-metal bonding using the metallic copper nanoparticles (Kobayashi *et al.* 2011, 2012, 2013a, b). According to those previous works, the bonding properties of metallic copper nanoparticles are strongly dependent on fabrication conditions such as species of raw copper salt, concentration of raw chemicals and reaction temperature. In the present work, concentration of hydrazine as a reducing reagent and reduction

temperature used in the synthesis of metallic-copper nanoparticles were focused on, and the effects of these factors on the morphology and the metal-metal bonding property of the nanoparticles were revealed.

2. Experimental

2.1 Chemicals

Copper-chloride dihydrate ($\text{CuCl}_2 \cdot 2\text{H}_2\text{O}$) (> 99%) and hydrazine monohydrate (> 98.0%) were used as a source of metallic-copper nanoparticles and a reducing reagent, respectively. The chemicals used for stabilizing particle colloid solutions were citric-acid monohydrate (> 99.5%) and cetyltrimethylammonium bromide (CTAB) (99%). All chemicals were purchased from Kanto Chemical Co., Inc. and used as received. Water used in all the preparations was prepared by ion-exchanging and distillation by water purifier (Yamato WG-250). The water was deaerated by bubbling with nitrogen gas for 30 min prior to preparation of various aqueous solutions.

2.2 Preparation

Metallic-copper nanoparticles were fabricated by reducing copper ions with hydrazine in aqueous solution, explained as follows. Freshly prepared hydrazine aqueous solution was added to aqueous solution of CuCl_2 , citric acid, and CTAB under vigorous stirring at reduction temperatures of 30-80°C. Initial concentrations of these chemicals were 0.01 M CuCl_2 , 0.1-1.0 M hydrazine, 0.0005 M citric acid and 0.005 M CTAB. The reduction time was 3 h. After the reduction, the obtained particles were washed by the following procedure (repeated several times): centrifugation at 10,000 rpm, removal of supernatant, addition of water and shaking of the mixture with a vortex mixer to disperse the particles.

2.3 Characterization

The nanoparticles were characterized by ultra-violet (UV-Vis) spectroscopy, transmission electron microscopy (TEM) and X-ray diffractometry (XRD). The UV-Vis extinction spectrum of the particle colloidal solution was measured using a Shimadzu UV-3101PC spectrophotometer. TEM photographs were taken with a JEOL JEM-2100 microscope operating at 200 kV. The TEM samples were prepared by dropping and evaporating the particle colloid on a collodion-coated copper grid. Number-averaged particle size and standard deviation of particle-size distribution were determined by measuring multiple particle diameters in the TEM images. XRD patterns of copper nanoparticles were acquired with a RAD-B X-ray diffractometer operating at 50 kV and 150 mA with $\text{CuK}\alpha$ radiation. To prepare the powder samples for the XRD measurement, the nanoparticles left after the final removal of supernatant were dried at room temperature for 24 h under vacuum.

The metal-metal bonding property of nanoparticle powder was investigated by the same set-up as used in our previous works, explained as follows. The same powder sample as that obtained for the XRD measurement was spread on a metallic-copper disc as a stage (with a diameter of 10 mm and a thickness of 5 mm). Then, a metallic-copper disc as a plate (with a diameter of 5 mm and a thickness of 2.5 mm) was put on the powder sample. The metallic copper discs sandwiching the

powder sample were compressed at 1.2 MPa under annealing in hydrogen at 400°C for 5 min with a Shinko Seiki vacuum reflow system. The bonding temperature was lower than a melting point of metallic copper (1085°C). The decrease in melting point of metallic material was expected to take place with the decrease in its size. In addition, the diffusion of components of metal was also expected to be accelerated by the compression. Bonding properties of the nanoparticles were evaluated in terms of shear strength required to separate the bonded disc and stage. The shear strength was measured with a Seishin SS-100KP bond tester at a shear rate of 30 mm/min. The measurement was performed only once for each sample. Because our research group has evaluated bonding properties for years, one measurement was regarded to be enough for obtaining data with accuracy in the present work. The disc surface was observed by scanning electron microscope (SEM), namely, a JEOL JSM-5600LV, after the shear strength was measured.

3. Results and discussion

3.1 Effect of hydrazine concentration

Photographs of the colloid solutions prepared at various hydrazine concentrations are shown in Fig. 1. In all the colloid solutions, the addition of hydrazine produced a reddish-brown color, which appeared to be due to surface plasmon resonance (SPR) of metallic copper nanoparticles (Singh *et al.* 2010, Niranjana and Chakraborty 2012, Xu *et al.* 2015), implying that metallic copper nanoparticles were produced. An example of their UV-Vis extinction spectra is shown in Fig. 2(a). A peak attributed to SPR of metallic Cu nanoparticles was detected at 589 nm, which supported the implication. TEM images of particles contained in the colloid solutions are shown in Fig. 3.

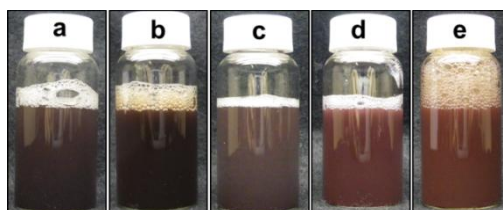


Fig. 1 Photographs of copper-particle colloid solutions prepared at hydrazine concentrations of (a) 0.2; (b) 0.4; (c) 0.6; (d) 0.8; and (e) 1.0 M. Reduction temperature was 30°C

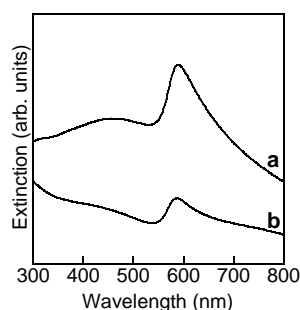


Fig. 2 Extinction spectra of copper-particle colloid solutions. The samples (a) and (b) were the same as the sample (a) in Fig. 1 and the sample (f) in Fig. 8, respectively

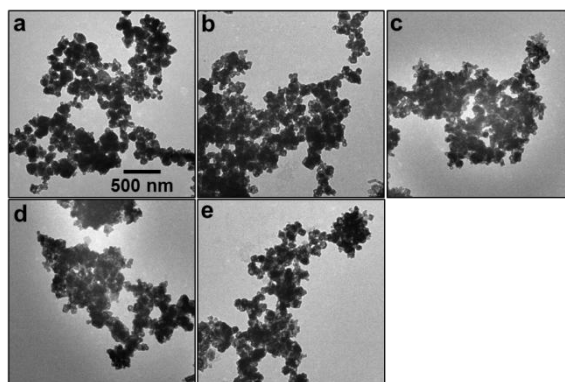


Fig. 3 TEM images of copper nanoparticles. Samples (a)-(e) were obtained from colloid solutions (a)-(e) shown in Fig. 1

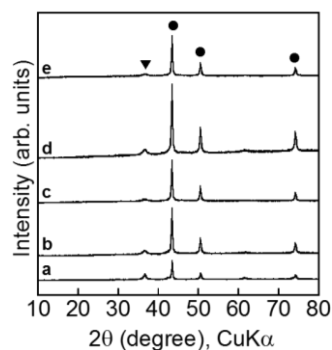


Fig. 4 XRD patterns of copper nanoparticles. Samples (a)-(e) were the same as those represented in Fig. 3. ●: metallic copper, and ▼: Cu_2O

Many quasi-angular particles were observed in all the samples. The particles sizes, namely, 162.9 ± 54.4 , 123.6 ± 28.9 , 120.0 ± 42.9 , 102.1 ± 29.0 and 87.2 ± 23.0 nm, corresponded to hydrazine concentrations of 0.2, 0.4, 0.6, 0.8 and 1.0 M, respectively. The particle size decreased with increasing hydrazine concentration. Addition of hydrazine increases ionic strength of the colloid solutions. It also increase reduction rate, or provides progress state of reduction. Since an increase in ionic strength compresses the double layer that forms on solid materials such as colloidal particles (Dickson *et al.* 2012, Sugimoto *et al.* 2014, Dimic-Misic *et al.* 2015), double-layer repulsion between particle nuclei becomes weak when their ionic strength is high, promoting aggregation of particle nuclei. As a result, large particles with high ionic strength are produced. On the other hand, an increase in reduction rate generates more particle nuclei. If each nuclei grows individually with no aggregation of nuclei, small particles will be produced because many particles are produced. The production of small particles was thus considered to take place more intensively when hydrazine concentration increases. XRD patterns of the particles are shown in Fig. 4. For all samples, three peaks, at 43.3, 50.4 and 74.1 degrees, respectively, were recorded. The peaks were attributed to the (111), (200) and (220) planes of cubic copper (JCPDS card No. 04-0836). For each sample, the peak detected at 36.5 degrees was assigned to Cu_2O (JCPDS card No. 05-0667), though its intensity was weaker than those of cubic copper. Application of the Scherrer equation

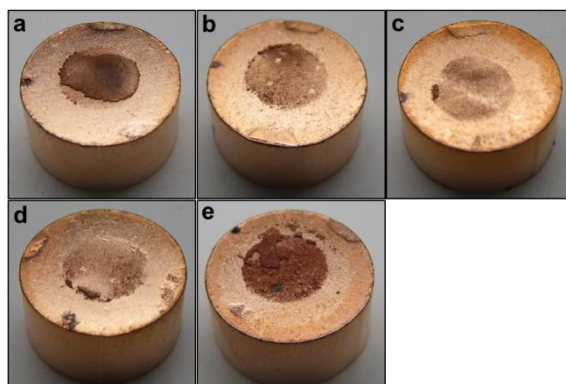


Fig. 5 Photographs of copper stages after measurement of shear strength. The powders used were the same as those represented in Fig. 3

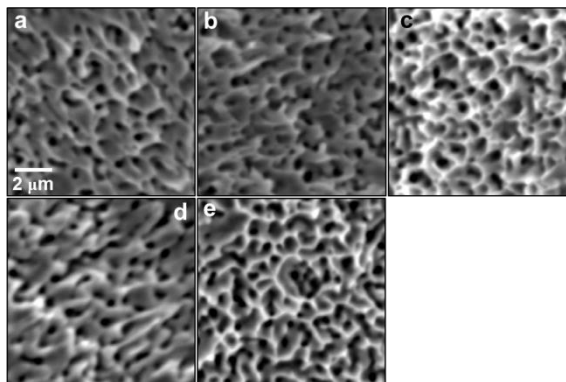


Fig. 6 SEM images of the copper stages shown in Fig. 5

the XRD line broadening of the 43.3° peak provided average metallic copper crystal sizes of 27.2, 26.1, 26.9, 24.7 and 25.9 nm for hydrazine concentrations of 0.2, 0.4, 0.6, 0.8 and 1.0 M, respectively. The crystal sizes at the hydrazine concentrations examined did not significantly differ, but they were smaller than the particle sizes. This result indicated that the metallic copper particles were polycrystalline.

Photographs of the copper stages after the measurement of shear strength are shown in Fig. 5. As for all the samples examined, reddish-brown products, which are clearly metallic copper, were observed on the stage. Surfaces that appeared to be the same as the copper stage were also observed in places. This observation indicated that the particle powder combined with the copper stage, which implied that the copper discs were strongly bonded. The reddish-brown product was also observed outside of the circle on the disc surface, especially in Fig. 4(e), because excess nanoparticle powder spread on metallic-copper stage stock out from metallic copper discs. The excess nanoparticle powder possibly made the disc surface rough, which lost luster of the disc surface. As a result, some regions of the disc surface appeared to have a color of black slightly. The nanoparticle surface should have been oxidized to also form CuO due to exposure in air containing oxygen, since CuO is also a chemically stable copper oxide. The XRD measurements did not reveal the existence of CuO, which implied that the amount of produced CuO was too low

to be detected by XRD. The surfaces of copper discs might have been also oxidized partially to form a slight layer of CuO. Accordingly, the black surfaces were speculated to be derived from CuO layers on nanoparticle surfaces and copper discs, and. Since further surface analyses such as XPS, XRD or EDS are required to prove the speculation provided with the observation, our research group would like to perform them in a future work. SEM images of the copper stages after the shear strength was measured are shown in Fig. 6. For all the samples, many dimples, accompanied by sharp tips, were observed on the surface. Tearing of strongly bonded metals with shearing stress forms the dimples in the bonded region (Morisada *et al.* 2010). These observations of dimples also confirmed strong bonding. Because solid materials should be separated at mechanically-weak point by shear stress, the point was considered to be the CuO layers in the present work. Nevertheless, the discs were bonded as strongly as the many dimples were produced. This indicated that the CuO layers were too thin to dominantly deteriorate the metal-metal bonding. Shear strength is plotted as a function of hydrazine concentration in Fig. 7. Shear strength was as high as ca. 25 MPa, corresponding to the strong bonding indicated by the naked-eye observation (Fig. 5) and the SEM observation (Fig. 6). It increased from 25.0 to 31.0 MPa with increasing hydrazine concentration from 0.2 to 0.8 M. The dimples observed for 0.8 M (Fig. 6(d)) were not significant compared to those for the hydrazine concentrations of 0.2-0.6 M (Figs. 6(a)-(c)). The discs also appeared to be brittle fractured by the shear stress. Brittle fracture often takes place in ceramics. The existence of Cu₂O brought about by the metal-metal bonding process taking on an aspect of ceramic bonding, resulted in the brittle fracture in the present work. The similar observation was also performed in our previous work on metal-metal bonding process using Cu₂O nanoparticles (Kobayashi *et al.* 2016). Some copper ions were probably unreduced at low hydrazine concentration, so they formed copper oxide. The copper oxide was reduced during the bonding in hydrogen gas. This reduction decreased the volume of particle powder, because oxygen was eliminated from the copper oxide through the reduction. This oxygen elimination resulted in production of voids in the particles during bonding. Because the voids did not contribute to the bonding, low shear strength was recorded at low hydrazine concentration. Another mechanism was also considered for explaining the increase in shear strength with the increase in hydrazine concentration from 0.2 to 0.8 M, as follows. As shown in Fig. 2, the particle size decreased with increasing hydrazine concentration. In our previous work, the shear strength tended to decrease with the particle size (Kobayashi *et al.* 2014). Its mechanism is as follows. Since small particles have large surface energy, they are apt to aggregate, resulting in an increase in apparent particle size. This increase causes a decrease in the contact area between the particle and Cu disc, which leads to the decrease in shear strength. This mechanism was also considered in the present work in the range of 0.2-0.8 M. However, the size of particles after drying the nanoparticles at room temperature for 24 h under vacuum has to be used for the discussion, since the particles after drying were used for the bonding. The particle size estimated from TEM observation should be different from that after the drying. The particle size after the drying is required for better understanding a precise mechanism on the bonding. Our research group would like to perform the measurement of particle size after the drying and to discuss the particle size as a parameter governing the shear strength in future work. Shear strength decreased to 24.5 MPa with increasing hydrazine concentration up to 1.0 M. Hydrazine concentration of 1.0 M was so high that unreacted hydrazine probably remained as an impurity in the solution. This unreacted hydrazine was removed from the particles with its sublimation or evaporation during bonding with annealing at the high temperature in hydrogen, and then also formed the voids in the particles. Consequently, shear strength decreased when hydrazine concentration increased to 1.0 M. Since the remaining of

unreacted hydrazine, on which information is quite important for understanding a mechanism on the decrease in shear strength, has not been proved, our research group also would like to characterize remained species in future work.

3.2 Effect of reduction temperature

Photographs of particle colloid solutions prepared at various reduction temperatures are shown in Fig. 8. For all the samples, the colloid solutions were all reddish brown, which also implied that metallic copper nanoparticles were produced. There were differences in coloration of reddish brown among the samples, though a precise mechanism on the differences is still unclear. The particles were highly dispersed, indicating that neither large particles nor aggregates forming sediment were produced at the reduction temperatures examined. An example of their UV-Vis extinction spectra is shown in Fig. 2(b). A peak attributed to SPR of metallic Cu nanoparticles was detected at 588 nm, which also supported the implication. TEM images of the particles in the colloid solutions are shown in Fig. 9. Many quasi-angular particles appeared in all samples. Their particles sizes were 120.0 ± 42.9 , 84.0 ± 18.8 , 97.4 ± 26.6 , 105.5 ± 25.0 , 133.6 ± 47.1 and 142.3 ± 40.0 nm for reduction temperatures of 30, 40, 50, 60, 70 and 80°C, respectively. When reduction temperature increased from 30 to 40°C, particle size decreased. The particle-size reduction rate was increased with increased reduction temperature, which generated many metallic copper nuclei. As a result, smaller particles were produced. Over 40°C, particle size increased with increasing reduction temperature. At high temperature, particles move quickly towards other primary particles, making it easy to coagulate the particles (Joshi 2006). Accordingly, after the particles aggregated and grew, high temperature caused them to coagulate. XRD patterns of the particles are show in

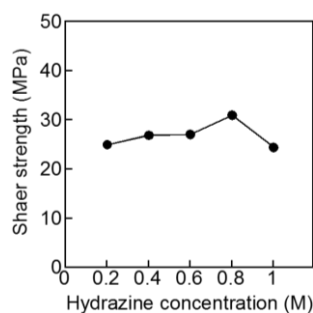


Fig. 7 Shear strength vs. hydrazine concentration.

The powders used were the particles shown in Fig. 3

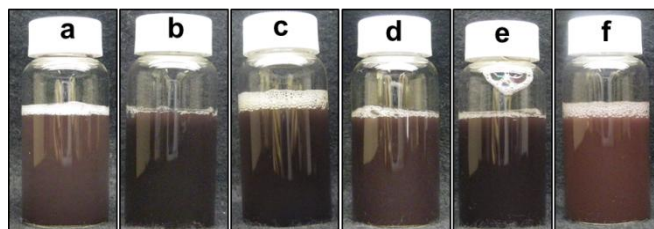


Fig. 8 Photographs of particle colloid solutions prepared at reduction temperatures of (a) 30; (b) 40; (c) 50; (d) 60; (e) 70; and (f) 80°C. Hydrazine concentration was 0.6 M

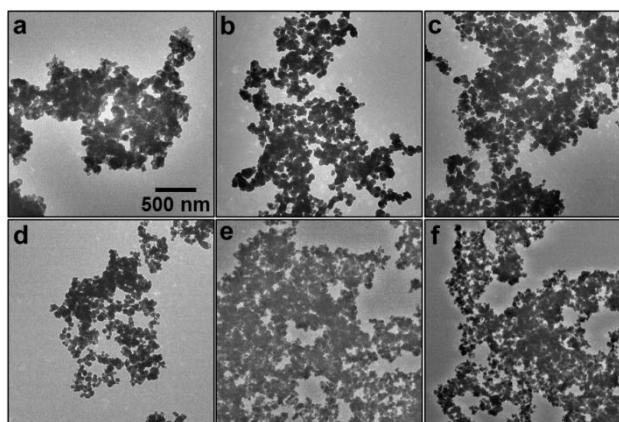


Fig. 9 TEM images of copper nanoparticles. Samples (a)-(f) were obtained from colloid solutions (a)-(e) shown in Fig. 8

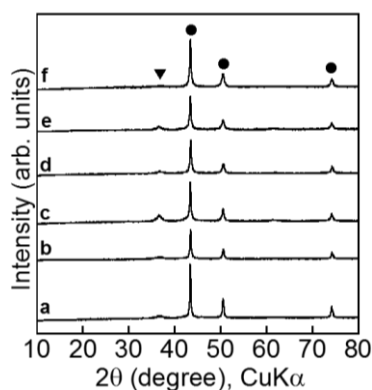


Fig. 10 XRD patterns of copper nanoparticles. Samples (a)-(e) were the same as those represented in Fig. 9. ●: metallic copper, and ▼: Cu₂O

Fig. 10. For all the samples, peaks attributed to the (111), (200) and (220) planes of cubic copper mainly appeared at 43.3, 50.4 and 74.1 degrees, and a faint peak assigned to Cu₂O also appeared at 36.5 degrees. No peaks due to CuO were detected, which implied that the amount of produced CuO was too low to be detected by XRD. According to the Scherrer equation applied to the XRD line broadening of the 43.3° peak, average metallic copper crystal sizes were estimated as 26.9, 24.0, 22.9, 21.9, 21.0 and 21.0 nm for reduction temperatures of 30, 40, 50, 60, 70 and 80°C, respectively: In other words, crystal size decreased with increasing reduction temperature, or crystal growth did not take place even with increasing reduction temperature. Increasing reduction temperature generated many metallic copper nuclei, as above-stated. The nuclei formed many crystallites, indicating production of small crystallites at high temperature. As discussed above, particle size increased with increasing reduction temperature over 40°C. Particles were thus speculated to grow following the production of crystallites with no dominant crystal growth. Photographs of the copper stages after the measurement of shear strength are shown in Fig. 11. Metallic copper surfaces (similar to that of the copper stage) with a reddish-brown color were observed on all the samples examined. These observations also implied that strong bonding took

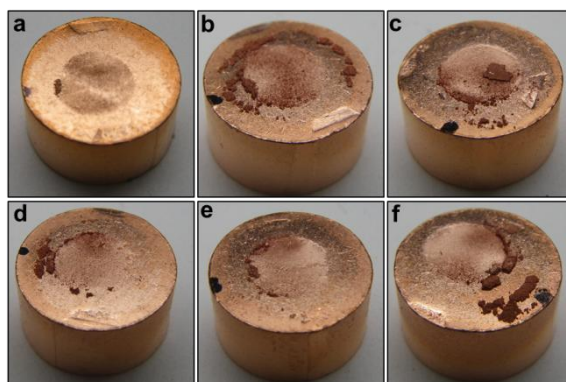


Fig. 11 Photographs of copper stages after measurement of shear strength. The powders used were the same as those represented in Fig. 9

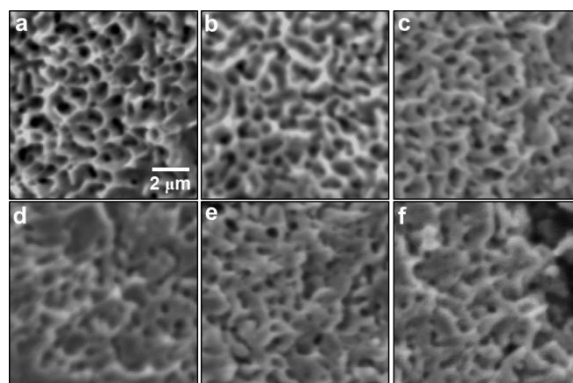


Fig. 12 SEM images of the copper stages shown in Fig. 11

place. The reddish-brown product was also observed on the disc surface outside of the circle especially in Figs. 11(b), (c), (d) and (f), because excess nanoparticle powder spread on metallic-copper stage also stock out from metallic copper discs. Some regions of the disc surface also appeared black slightly, which might have been derived from CuO layers on nanoparticle surfaces and copper discs. SEM images of the copper stages after shear strength was measured are shown in Fig. 12. For all the samples, the many dimples (accompanied by sharp tips) observed on the surface implied strong bonding. Dependence of shear strength on reduction temperature is plotted in Fig. 13. The shear strength was highest (40.0 MPa) at the highest reduction temperature (50°C). The shear strength of 40 MPa recorded in the present work was the highest among those obtained in our previous works on metallic Cu nanoparticles performed in several years (Kobayashi *et al.* 2011, 2012, 2013a). Shear strength is discussed on the basis of particle size as follows. Shear strengths were 20.7, 40.0, 20.0, 27.1, 16.7 and 24.3 MPa for particle sizes of 84.0, 97.4, 105.5, 120.0, 133.6 and 142.3 nm, respectively. That is, shear strength increased with decreasing particle size, though this tendency was rough. Particle size of the sample prepared with reduction temperature of 50°C was comparatively small. In the case of small particles, contact area between the particles and the copper discs was large. So, bonding of the sample with the large contact area was efficient at 50°C. Shear strength at reduction temperature of 40°C was smaller than that at

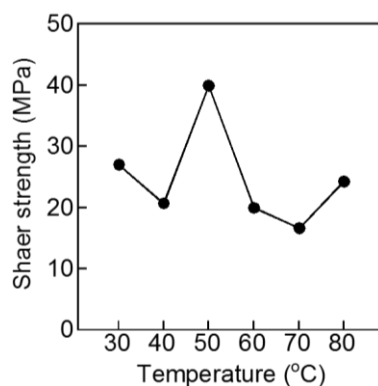


Fig. 13 Shear strength vs. reduction temperature.
The powders used were the particles shown in Fig. 9

50°C, although the particle size for 40°C was smaller than that for 50°C. It was previously reported (Maeda *et al.* 2014) that even though particle size was small, shear strength was not so high in a few cases. This low shear strength is possibly explained as follows. Small particles tend to aggregate because of their large surface energy, so apparent particle size increases. This tendency was also seen in the present work. Consequently, contact area between the particles with large apparent size and the metallic copper discs decreased, thereby decreasing shear strength.

4. Conclusions

A method for synthesising metallic copper nanoparticles in aqueous solution was proposed. As for this method, colloid solutions of metallic copper nanoparticles were prepared by reducing copper ions derived from CuCl_2 with hydrazine in the presence of citric acid and CTAB in water. At constant reduction temperature of 30°C, particle size decreased with increasing hydrazine concentration. The mechanism of this particle-size decrease was explained by the change in number of metallic-copper-particle nuclei, which is determined by the dependence of reduction rate on hydrazine concentration. The highest shear strength (31.0 MPa) was recorded at 0.8 M, because the reduction was completed and the amount of unreacted hydrazine was faint at 0.8 M. At constant hydrazine concentration of 0.6 M, particles with minimum particle size (84.0 ± 18.8 nm) were produced at 40°C. This result was explained in terms of both changes in number of metallic-copper-particle nuclei (determined by reduction rate) and collision frequency of particles based on movement of particles (which is dependent on temperature). Shear strength for 50°C was 40.0 MPa (that is, the largest among the samples examined). This result was explained in terms of the progress state of reduction, amount of impurity and particle size. Measurement of thermal conductivity has not been performed yet. Since information on the thermal conductivity is quite important for practical use of fillers in metal-metal bonding process, a study on metal-metal bonding is being awaited.

Acknowledgments

This work was partially supported by Hitachi, Ltd.

References

- Abtewa, M. and Selvaduray, G. (2000), "Lead-free solders in microelectronics", *Mater. Sci. Eng.*, **27**(5-6), 95-141.
- Argueta-Figueroa, L., Morales-Luckie, R.A., Scougall-Vilchis, R. and Olea-Mejía, O.F. (2014), "Synthesis, characterization and antibacterial activity of copper, nickel and bimetallic Cu-Ni nanoparticles for potential use in dental materials", *Prog. Nat. Sci.*, **24**(4), 321-328.
- Bai, J.G., Zhang, Z.Z., Calata, J.N. and Lu, G.Q. (2006), "Low-temperature sintered nanoscale silver as a novel semiconductor device-metallized substrate interconnect material", *IEEE Trans. Compon. Pack. Technol.*, **29**(3), 589-593.
- Darwish, S.M., Al-Habdanb, S. and Al-Tamimia, A. (2000), "A knowledge-base for electronics soldering", *J. Mater. Process. Technol.*, **97**(1-3), 1-9.
- Dickson, D., Liu, G., Li, C., Tachiev, G. and Cai, Y. (2012), "Dispersion and stability of bare hematite nanoparticles: Effect of dispersion tools, nanoparticle concentration, humic acid and ionic strength", *Sci. Total Environ.*, **419**, 170-177.
- Dimic-Misic, K., Hummel, M., Paltakari, J., Sixta, H., Maloney, T. and Gane, P. (2015), "From colloidal spheres to nanofibrils: Extensional flow properties of mineral pigment and mixtures with micro and nanofibrils under progressive double layer suppression", *J. Colloid Interf. Sci.*, **446**, 31-43.
- Duarte, L.I., Viana, F., Ramos, A.S., Vieira, M.T., Leinenbach, C., Klotz, U.E. and Vieira, M.F. (2012), "Diffusion bonding of gamma-TiAl using modified Ti/Al nanolayers", *J. Alloy. Compd.*, **536**(S1), S424-S427.
- Hashimoto, S., Werner, D. and Uwada, T. (2012), "Studies on the interaction of pulsed lasers with plasmonic gold nanoparticles toward light manipulation, heat management, and nanofabrication", *J. Photochem. Photobiol. C*, **13**(1), 28-54.
- Ide, E., Angata, S., Hirose, A. and Kobayashi, K.F. (2005), "Metal-metal bonding process using Ag metallo-organic nanoparticles", *Acta Mater.*, **53**(8), 2385-2393.
- Ishizaki, T., Satoh, T., Kuno, A., Tane, A., Yanase, M., Osawa, F. and Yamada, Y. (2013), "Thermal characterizations of Cu nanoparticle joints for power semiconductor devices", *Microelectron. Reliab.*, **53**(9-11), 1543-1547.
- Ji, F., Xue, S., Lou, J., Lou, Y. and Wang, S. (2012), "Microstructure and properties of Cu/Al joints brazed with Zn-Al filler metals", *Trans. Nonferrous Met. Soc. China*, **22**(2), 281-287.
- Ji, H., Li, L. and Li, M. (2015), "Low-temperature joining of Fe-based amorphous foil with aluminum by ultrasonic-assisted soldering with Sn-based fillers", *Mater. Design*, **84**, 254-260.
- Joshi, R.K. (2006), "pH and temperature dependence of particle size in $Pb_{1-x}Fe_xS$ nanoparticle films", *Solid State Commun.*, **139**(5), 201-204.
- Kikuchi, S., Nishimura, M., Suetsugu, K., Ikari, T. and Matsushige, K. (2001), "Strength of bonding interface in lead-free Sn alloy solders", *Mater. Sci. Eng. A*, **319-321**, 475-479.
- Kim, K.-S., Bang, J.-O. and Jung, S.-B. (2013), "Electrochemical migration behavior of silver nanopaste screen-printed for flexible and printable electronics", *Curr. Appl. Phys.*, **13**(S1), S190-S194.
- Kobayashi, Y., Shirochi, T., Yasuda, Y. and Morita, T. (2011), "Preparation of metallic copper nanoparticles in aqueous solution and their bonding properties", *Solid State Sci.*, **13**(3), 553-558.
- Kobayashi, Y., Shirochi, T., Yasuda, Y. and Morita, T. (2012), "Metal-metal bonding process using metallic copper nanoparticles prepared in aqueous solution", *Int. J. Adhes. Adhes.*, **33**, 50-55.
- Kobayashi, Y., Shirochi, T., Yasuda, Y. and Morita, T. (2013a), "Preparation of metallic copper nanoparticles by reduction of copper ions in aqueous solution and their metal-metal bonding properties", *Int. J. Phys. Nat. Sci. Eng.*, **7**(10), 150-153.
- Kobayashi, Y., Shirochi, T., Maeda, T., Yasuda, Y. and Morita, T. (2013b), "Microstructure of metallic copper nanoparticles/metallic disc interface in metal-metal bonding using them", *Surf. Interf. Anal.*, **45**(9), 1424-1428.
- Kobayashi, Y., Abe, Y., Maeda, T., Yasuda, Y. and Morita, T. (2014), "A Metal-metal bonding process using metallic copper nanoparticles produced by reduction of copper oxide nanoparticles", *J. Mater. Res.*

- Technol.*, **3**(2), 114-121.
- Kobayashi, Y., Maeda, T., Yasuda, Y. and Morita, T. (2016), "Metal-metal bonding process using cuprous oxide nanoparticles", *J. Mater. Res. Technol.*, **5**(4), 345-352.
- Kotadia, H.R., Howes, P.D. and Mannan, S.H. (2014), "A review: On the development of low melting temperature Pb-free solders", *Microelectron. Reliab.*, **54**(6-7), 1253-1273.
- Lee, K.S. and Kwon, Y.-N. (2013), "Solid-state bonding between Al and Cu by vacuum hot pressing", *Trans. Nonferrous Met. Soc. China*, **23**(2), 341-346.
- Lu, G.-Q., Yan, C., Mei, Y. and Li, X. (2015), "Dependence of electrochemical migration of sintered nanosilver on chloride", *Mater. Chem. Phys.*, **151**, 18-21.
- Maeda, T., Nakazawa, H., Kobayashi, Y., Yasuda, Y. and Morita, T. (2014), "Effects of reductant concentration and reduction temperature in synthesis of copper nanoparticles on their metal-metal bonding properties", *Sci. Lett.*, **8**(2) 1-9.
- Morisada, Y., Nagaoka, T., Fukusumi, M., Kashiwagi, Y., Yamamoto, M. and Nakamoto, M. (2010), "A low-temperature bonding process using mixed Cu-Ag nanoparticles", *J. Electron. Mater.*, **39**(8), 1283-1288.
- Murray, A.J., Jaroenapibal, P., Koene, B. and Evoy, S. (2006), "Sintering of silver nanoparticles for the formation of high temperature interconnect joints", *Mater. Res. Soc. Symp. Proc.*, **942**, 0942-W08-29.
- Nami, H., Halvae, A., Adgi, H. and Hadian, A. (2010), "Investigation on microstructure and mechanical properties of diffusion bonded Al/Mg₂Si metal matrix composite using copper interlayer", *J. Mater. Process. Technol.*, **210**(10), 1282-1289.
- Niranjan, M.K. and Chakraborty, J. (2012), "Synthesis of oxidation resistant copper nanoparticles in aqueous phase and efficient phase transfer of particles using alkanethiol", *Colloids Surf. A*, **407**, 58-63.
- Nishikawa, H., Hirano, T., Takemoto, T. and Terada, N. (2011), "Effects of joining conditions on joint strength of Cu/Cu joint using Cu nanoparticle paste", *Open Surf. Sci. J.*, **3**, 60-64.
- Noor, E.E.M., Sharif, N.M., Yew, C.K., Ariga, T., Ismail, A.B. and Hussain, Z. (2010), "Wettability and strength of In-Bi-Sn lead-free solder alloy on copper substrate", *J. Alloy. Compd.*, **507**(1), 290-296.
- Shi, F.G., Abdullah, M., Chungpaiboonpatana, S., Okuyama, K., Davidson, C. and Adams, J.M. (1999), "Electrical conduction of anisotropic conductive adhesives: effect of size distribution of conducting filler particles", *Mater. Sci. Semiconduct. Process.*, **2**(3), 263-269.
- Shibuta, Y. and Suzuki, T. (2010), "Melting and solidification point of fcc-metal nanoparticles with respect to particle size: A molecular dynamics study", *Chem. Phys. Lett.*, **498**(4-6), 323-327.
- Shiue, R.K., Tsay, L.W., Lin, C.L. and Ou, J.L. (2003), "The reliability study of selected Sn-Zn based lead-free solders on Au/Ni-P/Cu substrate", *Microelectron. Reliab.*, **43**(3), 453-463.
- Singh, M., Sinha, I., Premkumar, M., Singh, A.K. and Mandal, R.K. (2010), "Structural and surface plasmon behavior of Cu nanoparticles using different stabilizers", *Colloids Surf. A*, **359**(1-3), 88-94.
- Son, Y., Yeo, J., Ha, C.W., Lee, J., Hong, S., Nam, K.H., Yang, D.-Y. and Ko, S.H. (2012), "Application of the specific thermal properties of Ag nanoparticles to high-resolution metal patterning", *Thermochim. Acta*, **542**, 52-56.
- Sugimoto, T., Kobayashi, M. and Adachi, Y. (2014), "The effect of double layer repulsion on the rate of turbulent and Brownian aggregation: experimental consideration", *Colloids Surf. A*, **443**, 418-424.
- Tan, C.S., Lim, D.F., Ang, X.F., Wei, J. and Leong, K.C. (2012), "Low temperature Cu-Cu thermo-compression bonding with temporary passivation of self-assembled monolayer and its bond strength enhancement", *Microelectron. Reliab.*, **52**(2), 321-324.
- Tu, K.-N. (2007), *Solder Joint Technology*, Springer, New York, NY, USA.
- Wang, Z., Wang, H. and Liu, L. (2012), "Study on low temperature brazing of magnesium alloy to aluminum alloy using Sn-xZn solders", *Mater. Design*, **39**, 14-19.
- Weisman, C. (1976) *Welding Handbook*, Volume 1, (7th Edition), American Welding Society, MI, USA.
- Xu, L., Peng, J., Srinivasakannan, C., Chen, G. and Shen, A.Q. (2015), "Synthesis of copper nanocolloids using a continuous flowbased microreactor", *Appl. Surf. Sci.*, **355**, 1-6.
- Yan, J., Zou, G., Wu, A., Ren, J., Yan, J., Hu, A. and Zhou, Y. (2012a), "Pressureless bonding process using Ag nanoparticle paste for flexible electronics packaging", *Scr. Mater.*, **66**(8), 582-585.

- Yan, J., Zou, G., Wu, A., Ren, J., Hu, A. and Zhou, Y.N. (2012b), "Polymer-protected Cu-Ag mixed NPs for low-temperature bonding application", *J. Electron. Mater.*, **41**(7), 1886-1892.
- Yasuda, Y., Ide, E. and Morita, T. (2009), "Low-temperature bonding using silver nanoparticles stabilized by short-chain alkylamines", *Jpn. J. Appl. Phys.*, **48**(12R), 125004.
- Zhang, L. and Tu, K.N. (2014), "Structure and properties of lead-free solders bearing micro and nano particles", *Mater. Sci. Eng. R*, **82**, 1-32.

JL